

Relativistic unitary description of $\pi\pi$ scattering

M. A. Pichowsky, A. Szczepaniak, and J. T. Londergan

Department of Physics and Nuclear Theory Center, Indiana University, Bloomington, Indiana 47405

A unitary framework based on the Bakamjian-Thomas construction of relativistic quantum mechanics is used to describe two-pion scattering from threshold to 1400 MeV. The framework properly includes unitarity cuts for one-, two- and three-hadron states and provides an excellent description of the available data for $\pi\pi$ phase shifts and inelasticities. The role and importance of three-hadron cuts are calculated and discussed.

I. INTRODUCTION

A nonperturbative framework capable of describing the relativistic, coupled-channel scattering of hadrons is presented. The approach is based on a relativistic Hamiltonian formulation with model interactions introduced into the mass operator, and with few-body states implemented in a way that maintains the unitarity of the theory. The elementary degrees of freedom in the framework are finite-sized hadrons which provide a natural ultraviolet regularization, ensuring that the scattering amplitudes are finite.

The Hilbert space is truncated to include only one-, two- and three-body states. A central and novel feature of this framework is the explicit inclusion of both real and imaginary parts of scattering amplitudes arising from the opening of three-body channels. The proper handling of three-body unitarity cuts is crucial to gaining a deeper understanding of several well-known scattering systems; a good example is πN scattering in the P_{11} channel, which exhibits a significant inelasticity arising from the intermediate three-body $\pi\pi N$ state [1].

It presents a formidable challenge to develop a general, relativistic scattering framework to describe the final-state interactions between hadrons, that includes the effects of three-body unitarity cuts. Nonetheless, a practical framework which can treat hadron reactions beyond the lowest-order valence quark picture is clearly desirable. For example, the systematic analysis of hadron reactions in the baryon resonance region currently being conducted in Hall B at the Thomas Jefferson National Accelerator Facility (TJNAF) requires that such a framework be used to extract information about baryon resonances in this highly complex dynamical region. The framework developed herein is an attempt to construct a useful, relativistic framework capable of describing the nonperturbative, low-momentum transfer final-state interactions between hadrons in a unitary manner.

For the first application of the framework developed here, a simple model for $\pi\pi$ scattering is introduced and used to describe the S and P partial waves for energies

ranging from the two-pion threshold up to 1400 MeV. This system provides an excellent test for the framework. A relativistic treatment is quite important when dealing with particles as light as pions and the interplay between strong dynamics and chiral symmetry makes this system quite interesting. The $\pi\pi$ system is somewhat simpler than others, in that its study requires only a minimal complication from the proper implementation of relativistic spins, since both of the two-body states ($\pi\pi$ and $K\bar{K}$) involved are comprised of spin-0 particles. Another attractive aspect of applying the framework to $\pi\pi$ scattering is the relative wealth of experimental data for the isoscalar, S -wave channel.

One drawback with using $\pi\pi$ scattering as a touchstone may be that inelasticities due to *open* states of three or more particles, do not appear to be significant for this process; that is, the $\rho\pi\pi$ and $\pi\pi\pi\pi$ thresholds seem to have little impact on the S - and P -wave observables. The effects of the opening of these three- and four-body channels seem to be overwhelmed by the opening of the two-body $K\bar{K}$ channel. Nonetheless, several important aspects of the framework can be explored in an application to $\pi\pi$ scattering.

The isoscalar-scalar ($I = 0, J^{PC} = 0^{++}$) channel of $\pi\pi$ scattering has been a subject of numerous and extensive studies. The study of meson scattering in this low-energy region may be an ideal test of our understanding of the interplay between bound states in QCD and chiral dynamics. The region near $E = 1000$ MeV is perhaps most interesting, as it is dominated by the mixing between $\pi\pi$ and $K\bar{K}$ channels and the isoscalar-scalar $f_0(980)$ meson resonance. The nature of the $f_0(980)$ resonance, and the question of whether it is comprised of valence quarks or arises purely from meson scattering dynamics, has been addressed by many authors [2–8]. Above this energy region, three additional scalar meson resonances have been well established. These are referred to as the $f_0(1370)$, $f_0(1500)$ and the $f_0(1710)$. It is still unclear which of these should be considered as quark-antiquark bound states, glueballs or possibly resonances arising from dynamical effects of final-state interactions [9–13]. Thus, the isoscalar-scalar channel remains a source of great interest and mystery for meson phenomenology.

Although there have been previous studies which employ a framework similar to the one developed here, there are some important differences. Most studies of meson scattering dynamics are based on potential models (as is the framework developed here.) However, most other approaches typically include one- and two-particle channels only; that is, they include s -channel states and several two-particle channels, such as $\pi\pi$, $K\bar{K}$, $\sigma\sigma$, etc. They

either neglect the possibility of open three-particle channels altogether or only partially implement them. For example, in the model developed by the Julich group [14], the interaction potentials between two-particle channels, such as $\pi\pi$ - $\pi\pi$ or $\pi\pi$ - $K\bar{K}$ interactions are obtained using an instantaneous approximation of a meson-exchange model. Such instantaneous approximations generally do not account for absorptive effects due to the opening of three-body channels. Still, there is no question that the Julich model quite successfully describes the phase shifts and inelasticities of $\pi\pi$ scattering for S , P and D waves. Alternatively, the Krakow group [15] has developed a separable-potential model for $\pi\pi$ scattering. In their calculation, few-body dynamical effects are incorporated by including additional, *effective* two-body channels, such as a $\sigma\sigma$ channel [16]. Their model also obtains excellent results for the $\pi\pi$ phase shifts and inelasticities.

The outline of this article is as follows. In Sec. II, the relativistic scattering formalism employed herein is briefly discussed, beginning with a short proof of the covariance of observables calculated within this framework. Then, the integral equations that relate the one-, two- and three-body scattering T -matrices are provided.

In Sec. III, the framework is applied to a study of $\pi\pi$ scattering. The particle states that are included in the model are discussed, along with the necessary dynamical model parameters. The interactions employed in this study arise from the meson exchanges which couple states of various numbers of particles to each other. In our framework, these interactions arise from one-, two- and three-meson intermediate states which may exhibit production thresholds, resulting in absorptive contributions to the kernels and self-energies appearing in the Lippmann-Schwinger equations. A simple fitting procedure is shown to provide excellent agreement with data for $\pi\pi$ scattering phase shifts and inelasticities. Details of the relevant model dynamics that produce the various features observed in the resulting phase shifts and inelasticities are discussed. Then, it is shown that the numerical methods employed herein are sufficient to maintain the unitarity of the framework to better than one part in a million. Finally, in Sec. IV, the article is summarized and plans for future studies are presented.

II. RELATIVISTIC QUANTUM MECHANICAL FRAMEWORK

In this section, a relativistic Hamiltonian framework that provides a covariant unitary approach to the study of multichannel scattering is described. Lorentz symmetry is maintained by identifying the interactions with the mass operator (that is, the Hamiltonian in the overall center-of-momentum frame). It is shown in Ref. [17] that the complete set of Poincare generators can be constructed in a simple way that separates the internal dynamics from the center-of-momentum (CM) motion. In

Sec. II A a proof of the covariance of this approach is provided. Furthermore, Betz and Coester [18] show that such a framework can satisfy cluster separability. All of these features are desirable for the study of hadron scattering.

In Sec. II A, the Lorentz covariance of the framework is demonstrated and the fully-interacting mass operator \mathcal{M} is constructed. It is shown that the framework leads to Lorentz-invariant on-shell T -matrix elements $T(E, \mathbf{P})$ for colliding particles with total momentum \mathbf{P} and energy E ; that is, one finds $T(E, \mathbf{P}) = T(\sqrt{s})$ where $\sqrt{s} = \sqrt{E^2 - \mathbf{P}^2}$ is the invariant mass of the system.

The Poincare generators act on a Hilbert space which, in general, contains an infinite number of states. The Hilbert space is truncated to include only those states essential to describe the scattering system of interest within a particular energy range. Here, only one-, two- and three-particle states are maintained. Following this truncation, the operator form of the Lippmann-Schwinger equation can be written as a set of coupled integral equations. The input that determines the dynamics is given in terms of the matrix elements of a model potential V . Once these are provided, the full scattering problem is solved in a straightforward manner.

A. Relativistic covariance

A simple realization of the Poincare algebra for an interacting system of a finite number of constituents is given by the Bakamjian-Thomas construction [17]. This approach has the advantage of providing a Lorentz-covariant generalization for a large class of noncovariant microscopic models, such as the constituent quark model. In principle, a noncovariant microscopic model could be used to obtain matrix elements of the underlying elementary hadronic potentials V . In this case, one might consider this framework as a means to extend the original noncovariant model dynamics, allowing for a Lorentz-covariant treatment of scattering phenomena.

The explicit construction of the Poincare algebra proceeds as follows. Starting from a system of *noninteracting* particles, described by their coordinates \mathbf{x}_a , momenta \mathbf{p}_a , spins \mathbf{s}_a , and masses m_a , the Poincare generators are

$$\begin{aligned} H &= \sum_a \mathcal{E}(m_a, \mathbf{p}_a) = \sum_a \sqrt{m_a^2 + \mathbf{p}_a^2}, \\ \mathbf{P} &= \sum_a \mathbf{p}_a, \\ \mathbf{J} &= \sum_a \mathbf{x}_a \times \mathbf{p}_a + \mathbf{s}_a, \\ \mathbf{K} &= \sum_a \frac{1}{2} \{ \mathbf{x}_a, \mathcal{E}(m_a, \mathbf{p}_a) \} - \frac{\mathbf{s}_a \times \mathbf{p}_a}{\mathcal{E}(m_a, \mathbf{p}_a) + m_a}. \end{aligned} \quad (2.1)$$

Here, H and \mathbf{P} are the total free energy and linear momentum of the system, \mathbf{J} and \mathbf{K} are the total angular momentum and boost operators, respectively. The

relative coordinates \mathbf{r}_a , relative momenta \mathbf{k}_a , center-of-momentum (CM) spins \mathbf{s}'_a , and the CM coordinates \mathbf{R}_{cm} , total momentum \mathbf{P}_{cm} , and total spin \mathbf{S}_{cm} , are introduced via the Gartenhaus-Schwartz transformation which allows a separation of the *internal* dynamics and CM motion. In terms of these new variables, the Poincare generators are given by

$$\begin{aligned} H &= \sqrt{\mathbf{P}^2 + \mathcal{M}^2(\mathbf{k}_1, \mathbf{k}_2, \dots)}, \\ \mathbf{P} &= \mathbf{P}_{cm}, \\ \mathbf{J} &= \mathbf{R}_{cm} \times \mathbf{P}_{cm} + \mathbf{S}_{cm}, \\ \mathbf{K} &= \frac{1}{2} \{ \mathbf{R}_{cm}, H \} - \frac{\mathbf{S}_{cm} \times \mathbf{P}_{cm}}{H + \mathcal{M}(\mathbf{k}_1, \mathbf{k}_2, \dots)}, \end{aligned} \quad (2.2)$$

with the constraints,

$$\begin{aligned} \sum_a m_a \mathbf{r}_a &= 0, \\ \sum_a \mathbf{k}_a &= 0, \\ \mathbf{S}_{cm} - \left(\sum_a \mathbf{r}_a \times \mathbf{k}_a + \mathbf{s}'_a \right) &= 0. \end{aligned} \quad (2.3)$$

In Eq. (2.2), the quantity $\mathcal{M} = \mathcal{M}(\mathbf{k}_1, \mathbf{k}_2, \dots)$ is referred to as the *free* invariant mass in the Schrödinger picture. The internal momenta \mathbf{k}_a are related to the individual particle momenta \mathbf{p}_a via a free Lorentz transformation to the CM frame,

$$\begin{aligned} \mathbf{k}_a &= \Lambda(\mathbf{k}_a \leftarrow \mathbf{p}_a) \mathbf{p}_a \\ &= \mathbf{p}_a + \frac{\mathbf{p}_a \cdot \mathbf{P}}{\mathcal{M}(\mathcal{M} + H)} \mathbf{P} - \frac{\mathcal{E}(m_a, \mathbf{p}_a)}{\mathcal{M}} \mathbf{P} \end{aligned} \quad (2.4)$$

and the CM frame spins \mathbf{s}'_a are related to the individual spins \mathbf{s}_a via a Wigner rotation corresponding to the product of Lorentz boosts $R = \Lambda(0 \leftarrow \mathbf{p}_a) \Lambda(\mathbf{p}_a \leftarrow \mathbf{k}_a) \Lambda(\mathbf{k}_a \leftarrow 0)$, leading to

$$\mathbf{s}'_a = D^{(s)}(R) \mathbf{s}_a D^{(s)}(R)^*. \quad (2.5)$$

Interactions are incorporated into the Poincare generators by the addition of a term in the free mass operator,

$$\mathcal{M} \rightarrow \mathcal{M}_I(\mathbf{r}_a, \mathbf{k}_a, \mathbf{s}'_a) = \mathcal{M} + V. \quad (2.6)$$

Thus, transforming the free Hamiltonian H into the interacting Hamiltonian H_I ,

$$\begin{aligned} H &\rightarrow H_I = H + W, \\ W &= \sqrt{\mathcal{M}_I^2 + \mathbf{P}^2} - \sqrt{\mathcal{M}^2 + \mathbf{P}^2}. \end{aligned} \quad (2.7)$$

This replacement preserves the canonical commutation relations, provided $V = V(\mathbf{r}_a, \mathbf{k}_a, \mathbf{s}'_a)$ is a function of internal coordinates only and is invariant under rotations $[V, \mathbf{J}] = [V, \mathbf{S}_{cm}] = 0$. For example, consider the case for which the elementary interaction is a Yukawa-type

three-meson vertex. The matrix elements of the three-meson interaction vertex would be given by $\langle a|V|bc \rangle$ and would only depend on the internal variables associated with the CM frame where $\mathbf{p}_a = \mathbf{p}_b + \mathbf{p}_c = 0$. Of course, these internal variables can be expressed in terms of the individual particle momenta in another frame by using the boost relations analogous to Eqs. (2.4) and (2.5).

Within this framework, the Lorentz covariance of observables may be demonstrated from the following considerations. Construct an invariant \mathcal{T} -matrix which satisfies a *Lorentz-invariant* Lippmann-Schwinger equation (LSE),

$$\mathcal{T} = \mathcal{V} + \mathcal{V} \mathcal{G} \mathcal{T}, \quad (2.8)$$

with an invariant interaction \mathcal{V} ,

$$\begin{aligned} \mathcal{V} &= H_I^2 - H^2 \\ &= (\mathbf{P}^2 + \mathcal{M}_I^2) - (\mathbf{P}^2 + \mathcal{M}^2) \\ &= W^2 + HW + WH \\ &= V^2 + \mathcal{M}V + V\mathcal{M}, \end{aligned} \quad (2.9)$$

and an invariant propagator \mathcal{G} for scattering energy E , given by

$$\begin{aligned} \mathcal{G} &= (E^2 - H^2 + i\epsilon)^{-1} \\ &= (E^2 - \mathbf{P}^2 - \mathcal{M}^2 + i\epsilon)^{-1}. \end{aligned} \quad (2.10)$$

Since \mathcal{V} is independent of the CM momentum \mathbf{P} and the scattering energy E , one may rewrite the scattering energy $E = \sqrt{s + \mathbf{P}^2}$, in terms of a new variable s , referred to as the invariant mass squared. From Eq. (2.10), one observes that the propagator $\mathcal{G}(s)$ is a function of the invariant mass squared only, and one concludes that the LSE (2.8) depends only on the invariant mass squared s . It follows that the resulting \mathcal{T} -matrix, $\mathcal{T}(\sqrt{s})$ depends only on the invariant mass squared s .

It is possible to relate the *on-shell* matrix elements of this invariant \mathcal{T} -matrix to the *on-shell* matrix elements of a T -matrix that is the solution of a non-invariant LSE with the interaction potential W ,

$$T(E, \mathbf{P}) = W + W G(E) T(E, \mathbf{P}), \quad (2.11)$$

where $G(E) = (E - H + i\epsilon)^{-1}$. The relation between the on-shell matrix elements is given by

$$\mathcal{T}(\sqrt{s}) = 2\sqrt{s + \mathbf{P}^2} T(E, \mathbf{P}), \quad (2.12)$$

which can be demonstrated term by term by expanding the *on-shell* matrix elements of \mathcal{T} in powers of the potential V ,

$$\begin{aligned} \mathcal{T} &= \mathcal{V} + \mathcal{V} \mathcal{G}(E) \mathcal{V} + O(V^3) \\ &= W^2 + 2EW \\ &\quad + W(E + H) \frac{1}{E^2 - H^2 + i\epsilon} (E + H)W + O(V^3) \\ &= 2EW + 2EW \frac{1}{E - H + i\epsilon} W + O(V^3) \\ &= 2ET(E, \mathbf{P}). \end{aligned}$$

In this article, calculations are carried out in the CM frame for which $E = \sqrt{s}$, then the interaction potential $W = \mathcal{M}_I - \mathcal{M} = V$, and the relevant LSE is

$$T(E) = V + V G(E) T(E), \quad (2.13)$$

where $T(E) = T(E, \mathbf{P} = 0)$. In the CM frame, one finds

$$\mathcal{T}(\sqrt{s}) = 2\sqrt{s} T(\sqrt{s}). \quad (2.14)$$

Thus, the on-shell matrix elements of the solution $T(E = \sqrt{s})$ of the non-invariant LSE in Eq. (2.13) are related by Eq. (2.14) to the on-shell matrix elements of the solution $\mathcal{T}(\sqrt{s})$ of the invariant LSE of Eq. (2.8). It follows that observables calculated from Eq. (2.13) are equivalent to those calculated from a Lorentz-invariant theory.

B. Coupled Lippmann-Schwinger Equations

In the above framework, the particle dynamics are given in the center-of-momentum (CM) frame where $\mathbf{P} = 0$ by the invariant mass operator,

$$\mathcal{M}_I = \mathcal{M} + V. \quad (2.15)$$

The quantity \mathcal{M} , introduced in Eq. (2.2), is the *free* invariant mass in the Schrödinger picture and V is the elementary hadron interaction potential.

The probability amplitude for observing an N -body state $|\beta\mathbf{Q}\rangle$ with total momentum \mathbf{Q} , given an initial N -body state $|\alpha\mathbf{P}\rangle$ with total momentum \mathbf{P} , is given by the S -matrix element $\langle\beta\mathbf{Q}|S(E)|\alpha\mathbf{P}\rangle$. The T -matrix $T(E, \mathbf{P})$ is defined by the Lippmann-Schwinger equation (LSE) of Eq. (2.13) and determines the on-shell S -matrix elements,

$$\langle\beta\mathbf{Q}|S(E)|\alpha\mathbf{P}\rangle = \langle\beta\mathbf{Q}|\alpha\mathbf{P}\rangle - 2\pi i \delta(\mathcal{E}(\mathcal{M}_\beta, \mathbf{Q}) - \mathcal{E}(\mathcal{M}_\alpha, \mathbf{P})) \langle\beta\mathbf{Q}|T(E, \mathbf{P})|\alpha\mathbf{P}\rangle, \quad (2.16)$$

where $\mathcal{E}(\mathcal{M}_\alpha, \mathbf{P}) = \sqrt{\mathcal{M}_\alpha^2 + \mathbf{P}^2}$.

The potential V and the T -matrix describe all interactions between the various channels, including channels with differing numbers of particles. In general, they do not conserve particle number. Therefore, the LSE of Eq. (2.13) represents an countably infinite system of coupled-channel equations which couple states of different numbers of particles.

This infinite system of coupled equations may be simplified by truncating the Hilbert space to include only a finite number of states that are expected to contribute substantially to a given reaction. For the purposes of this study, the Hilbert space is restricted to contain a finite number of one-, two-, and three-particle states. Furthermore, the particles are assumed to be of finite spatial extension, thereby providing an ultraviolet regularization to the theory. With these restrictions, the LSE of Eq. (2.13) reduces to a closed system of integral equations which may be solved exactly. Of course, one

drawback of such a truncation is that some symmetries, such as crossing symmetry, which require the inclusion of many-particle states may be lost. The addition of states with a higher number of particles, such as four-particle states, can in principle be included in a straightforward manner but the resulting set of equations would be far more complicated than that studied here.

The main objective of this work is to develop a framework for handling up to three-body channels in a fully unitary fashion, by including effects beyond their contribution to the real part of the effective, two-body potentials. The intended application is the description of soft final-state interactions in hadron production processes. Such processes are distinguished by their strong couplings and low momentum transfers. For this reason, composite hadrons (mesons and/or baryons) are chosen as the fundamental degrees of freedom rather than quarks and gluons.

The truncation of the Hilbert space to contain only one-, two- and three-hadron states may be sufficient since, in many applications, states with higher numbers of hadrons contribute very little to two-hadron elastic scattering amplitudes. This suppression arises because many-hadron intermediate states typically have a large invariant mass, which appears in the denominator of the Green function G , tending to weaken its contribution. Interestingly, this suppression of higher-order Hilbert space states is also observed in some quantum field theoretical frameworks. In a study of the pion-loop contribution to the ρ -meson self-energy and charge radius, based on a phenomenological application of the Dyson-Schwinger equations of QCD [19], the covariant, quantum field theoretic expression for the ρ -meson self-energy was separated into the various time orderings and their relative importance calculated. The time orderings include contributions arising from $\pi\pi$ and $\rho\rho\pi\pi$ intermediate states, as well as others. In this calculation, it was shown that terms associated with the two-pion intermediate state contributed more than 95% of the total, while the four-hadron states contributed less than 5%. Thus, one expects that a truncation scheme which neglects states with four or more hadrons should provide a reasonable description of the residual strong interactions between mesons and baryons.

The matrix elements of the potential V describe the couplings between hadrons that arise from the underlying QCD dynamics of quarks and gluons. Color confinement requires that all physical particle thresholds are associated with the colorless hadron states. It follows that the matrix elements of the potential V are real. In this framework, all of the analytic structure of the T -matrix necessarily arises from the color-singlet hadron poles and branch cuts which result from the LSE of Eq. (2.13).

Once the Hilbert space has been truncated to include only one-, two- and three-particle states, Eq. (2.13) is expanded and rewritten in a simpler form by labeling each of the Hilbert space operators with subscripts indicating the numbers of particles they act on. The potential V is

$$V = \begin{pmatrix} \text{---}\times\text{---} & \text{---}\text{C} & 0 \\ \text{---}\text{C} & \text{---}\times\text{---} + \text{---}\text{X} & \text{---}\text{U} + \text{---}\text{Z} \\ 0 & \text{---}\text{U} + \text{---}\text{Z} & 0 \end{pmatrix}$$

FIG. 1. Schematic diagram of the interaction potential matrix V of Eq. (2.18).

of the form

$$V = \begin{pmatrix} V_{11} & V_{12} & V_{13} \\ V_{21} & V_{22} & V_{23} \\ V_{31} & V_{32} & V_{33} \end{pmatrix}. \quad (2.17)$$

The part of the potential associated with the coupling of a one-particle state to a two-particle final state is denoted V_{21} . The resulting system of integral equations can be solved formally in a straightforward manner.

It is important to note that each matrix element of the potential V in Eq. (2.17) is itself a matrix, since it may contain interactions between any number of different particle channels. That is, matrix elements of the form V_{21} describe the couplings of any one-particle state with any two-particle state. The number of one-, two-, and three-particle states one wishes to include depends on the specific application. For the application to $\pi\pi$ scattering considered in Sec. III, a further simplification is made by assuming an absence of fundamental interactions in V connecting one-particle states to three-particle states, and three-particle states to three-particle states. Then, the potential V takes a simpler form,

$$V = \begin{pmatrix} V_{11} & V_{12} & 0 \\ V_{21} & V_{22} & V_{23} \\ 0 & V_{32} & 0 \end{pmatrix}, \quad (2.18)$$

and is shown schematically in Fig. 1.

The neglected terms $V_{13} = V_{31}^\dagger$ are associated with energy-independent transitions between one-particle and three-particle states. When such terms are neglected the only way in which a one-body state can decay into a three-body state is through a multiple-step process involving a two-body intermediate state.

In setting the term $V_{33} = 0$, several possible elementary interactions have been neglected. First, V_{33} describes direct energy-independent couplings between two three-body states, as well as interactions in which two of the particles interact while the third particle is a spectator. Such terms may be important. One might argue that it is inconsistent to include direct two-body interactions in V_{22} , but neglect the analogous two-body (plus spectator) interactions in V_{33} . Nonetheless, in this work such terms are ignored. The significance and role of these interactions will be addressed in future studies.

In the truncated Hilbert space, the free Green function is a diagonal matrix

$$\begin{aligned} \boxed{\Sigma} &= \text{---}\times\text{---} + \text{---}\text{C} + \text{---}\text{C} \\ \boxed{K} &= \text{---}\text{X} + \text{---}\text{C} + \text{---}\text{C} \end{aligned}$$

FIG. 2. Schematic diagram of the two-particle self-energy Σ , and the two-particle kernel K , as defined in Eq. (2.21).

$$G = \begin{pmatrix} G_1 & 0 & 0 \\ 0 & G_2 & 0 \\ 0 & 0 & G_3 \end{pmatrix}, \quad (2.19)$$

and the T -matrix is

$$T = \begin{pmatrix} T_{11} & T_{12} & T_{13} \\ T_{21} & T_{22} & T_{23} \\ T_{31} & T_{32} & T_{33} \end{pmatrix}. \quad (2.20)$$

In the CM frame, each submatrix G_1 , G_2 or G_3 in Eq. (2.19) is itself diagonal since our hadron states form a complete, orthogonal set of eigenstates of the free invariant mass operator \mathcal{M} .

Upon insertion of these forms for V , G and T from Eqs. (2.18), (2.19) and (2.20) into the LSE (2.13), one may formally solve this system of integral equations. It is convenient to consider the combination of terms $V_{22} + V_{23}G_3V_{32}$, which appears frequently in our formalism. These terms play an important role and so are collected and rewritten as the sum of Σ and K ,

$$\Sigma + K \equiv V_{22} + V_{23}G_3V_{32}. \quad (2.21)$$

These are referred to as the *two-particle self-energy* Σ , and the *two-particle kernel* K . These terms are defined such that the matrix elements of the two-particle self-energy Σ contain only terms proportional to a δ -function in the *relative* momentum of the two-particle state. Consequently, matrix elements of the two-particle kernel K contain all contributions that are *not* proportional to a δ -function in the relative momentum.

The two-particle self-energy and kernel are depicted schematically in Fig. 2. In the following, it will become apparent that Σ and K are the central elements of the framework, from which all other quantities are obtained. In fact, *all* effects due to three-particle intermediate states can be traced back to these two amplitudes.

One defines the *dressed* one- and two-particle Green functions in the usual manner as

$$\tilde{G}_1 = (G_1^{-1} - \Pi)^{-1}, \quad (2.22)$$

$$\tilde{G}_2 = (G_2^{-1} - \Sigma)^{-1}. \quad (2.23)$$

They are defined in terms of the two-body self-energy Σ and the one-body self-energy Π , where

$$\Pi = V_{11} + V_{12}\tilde{G}_2\tilde{V}_{21}, \quad (2.24)$$

$$\begin{aligned} \tilde{V}_{21} &= V_{21} + K\tilde{G}_2\tilde{V}_{21}, \\ &= (1 - K\tilde{G}_2)^{-1}V_{21}. \end{aligned} \quad (2.25)$$

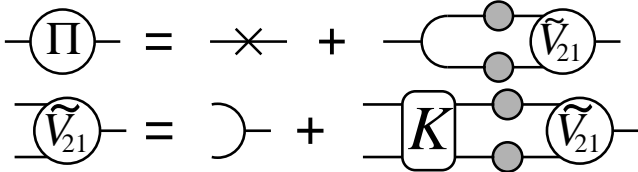


FIG. 3. Schematic diagram of the integral equations for the one-body self-energy Π and the dressed vertex \tilde{V}_{21} . These diagrams depict the expressions in (2.24) and (2.25).

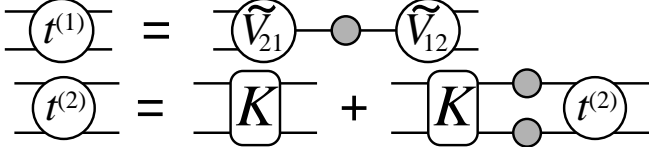


FIG. 4. Schematic diagram of the scattering amplitudes $t^{(1)}$ and $t^{(2)}$ which enter into the two-particle scattering matrix elements. These diagrams depict the expressions in Eqs. (2.27) and (2.28).

These quantities are shown schematically in Fig. 3.

The solution for the two-particle scattering T -matrix can be written as

$$T_{22} = G_2^{-1} \tilde{G}_2 (t^{(1)} + t^{(2)}) \tilde{G}_2 G_2^{-1} + G_2^{-1} \tilde{G}_2 \Sigma, \quad (2.26)$$

where

$$t^{(1)} = \tilde{V}_{21} \tilde{G}_1 \tilde{V}_{12}, \quad (2.27)$$

$$\begin{aligned} t^{(2)} &= K + K \tilde{G}_2 t^{(2)}, \\ &= (1 - K \tilde{G}_2)^{-1} K. \end{aligned} \quad (2.28)$$

These two scattering amplitudes are shown schematically in Fig. 4. Briefly, the contributions to the two-body scattering amplitude T_{22} that proceed through one-body channels are denoted $t^{(1)}$, while contributions that don't proceed through one-body channels are denoted $t^{(2)}$; both $t^{(1)}$ and $t^{(2)}$ contain the effects of the two- and three-body singularities, but only $t^{(1)}$ contains one-body singularities.

The matrix elements for the *dressed* Green function \tilde{G}_2 defined by Eq. (2.23) are given by

$$\tilde{G}_{\beta\alpha}(p, E) = \left(\delta_{\alpha\beta} (E - \mathcal{M}_{\alpha_{12}}(p) + i\epsilon) - \Sigma_{\alpha\beta}(p, E) \right)^{-1}. \quad (2.29)$$

One can collect the terms from Eq. (2.21) contributing to the two-body self-energy $\Sigma_{\beta\alpha}$, and organize them into the following sum,

$$\Sigma = \delta\Sigma + V_{23}^{(1)} G_3 V_{32}^{(1)} + V_{23}^{(2)} G_3 V_{32}^{(2)}. \quad (2.30)$$

Here, the superscript (i) refers to the diagram in which the i^{th} particle in the two-body state emits and subsequently re-absorbs the particle γ_3 . The term $\delta\Sigma$ is identified with the part of the potential V_{22} that is proportional to a Dirac δ -function in the relative two-body momentum. (All other terms that appear in Eq. (2.21) but

which do not appear in Σ in Eq. (2.30), are part of the two-body kernel K .)

Upon inserting a complete set of three-body states into Eq. (2.30) and evaluating the resulting expressions in the overall CM frame with $\mathbf{P} = 0$, one obtains

$$\begin{aligned} \Sigma_{\beta\alpha}^{(1)}(p, E) &= \sum_{\gamma_{13}} \int_0^\infty dk_{13} \frac{a_{\gamma_{13}}(k_{13}, p)}{2\sqrt{\mathcal{E}(m_{\beta_1}, p)\mathcal{E}(m_{\alpha_1}, p)}} \\ &\times V_{\beta_1\gamma_{13}}(k_{13}) G_\gamma(p, k_{13}, E) V_{\gamma_{13}\alpha_1}(k_{13}), \end{aligned} \quad (2.31)$$

where $\Sigma^{(i)} = V_{23}^{(i)} G_3 V_{32}^{(i)}$. A similar expression is obtained for $\Sigma_{\beta\alpha}^{(2)}(p, E)$. The momentum integration is over the relative momentum k_{13} between the first and third particles of the three-body intermediate state, J is the total angular momentum of the system, the sum is over all three-body states γ , and the three-body Green function is

$$G_\gamma(p, k_{13}, E) = \frac{1}{E - \mathcal{M}_{\gamma_{123}}(p, k_{13}) + i\epsilon}. \quad (2.32)$$

For brevity the ubiquitous two-body phase space factor,

$$a_{\gamma_{13}}(k_{13}, p) = \frac{k_{13}^2}{(2\pi)^3} \frac{\rho_{\gamma_{13}}(k_{13})}{2\mathcal{E}(\mathcal{M}_{\gamma_{13}}(k_{13}), p)}, \quad (2.33)$$

and two-body Jacobian

$$\rho_{\gamma_{13}}(k_{13}) = \frac{\mathcal{M}_{\gamma_{13}}(k_{13})}{2\mathcal{E}(m_{\gamma_1}, k_{13})\mathcal{E}(m_{\gamma_3}, k_{13})}, \quad (2.34)$$

are introduced. The expression in Eq. (2.31) for the two-body self-energy $\Sigma_{\beta\alpha}^{(1)}(p, E)$ is depicted in Fig. 5. The two-body self-energy $\Sigma_{\beta\alpha}(p, E)$ is then the sum,

$$\Sigma_{\beta\alpha}(p, E) = \delta\Sigma_{\beta\alpha}(p) + \Sigma_{\beta\alpha}^{(1)}(p, E) + \Sigma_{\beta\alpha}^{(2)}(p, E), \quad (2.35)$$

where the counter term is chosen to be

$$\delta\Sigma_\alpha(p) = - \left(\Sigma_\alpha^{(1)}(p, E) + \Sigma_\alpha^{(2)}(p, E) \right)_{E=\mathcal{M}_{\alpha_{12}}(p)}. \quad (2.36)$$

This is necessary and sufficient to ensure unitarity and that the stable two-body system α_{12} is observed asymptotically with the invariant mass $\mathcal{M}_{\alpha_{12}}(p)$. Evaluation of the two-body self-energy $\Sigma_\alpha(p, E)$ requires calculating the imaginary part and a principal part of the integral in Eq. (2.31). For energies E above a three-body threshold, these integrals encounter poles in the three-body Green function $G_\gamma(\mathbf{p}, \mathbf{k}_{13}, E)$ for values of the relative momentum $k_{13} = k_{0\gamma}$, where $k_{0\gamma}$ satisfies the relation $\mathcal{M}_{\gamma_{123}}(p, k_{0\gamma}) = E$.

From Eq. (2.24), one obtains an expression for the one-body self-energy in the CM frame,

$$\begin{aligned} \Pi_\alpha(E) &= \delta\Pi_\alpha + \frac{1}{2m_{\alpha_1}} \sum_{\gamma_{12}} \int_0^\infty dk a_{\gamma_{12}}(k, 0) \\ &\times V_{\alpha_1\gamma_{12}}(k) \tilde{G}_\gamma(k, E) \tilde{V}_{\gamma_{12}\alpha_1}(k, E). \end{aligned} \quad (2.37)$$

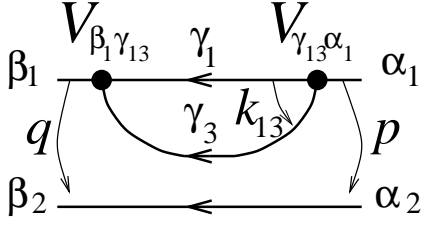


FIG. 5. Diagram depicting one of the contributions to the two-body self-energy $\Sigma_{\beta\alpha}^{(1)}(p, E)$ given in Eq. (2.31). Shown here, particle α_1 decays into particles γ_1 and γ_3 , and these subsequently recombine to form particle β_1 . The relative momentum between the intermediate particles γ_1 and γ_3 is k_{13} , the relative momentum of the incoming state $|\alpha_1 \mathbf{p}_1 \mathbf{p}_2\rangle$ is p , and relative momentum of the outgoing state $|\beta_1 \mathbf{q}_1 \mathbf{q}_2\rangle$ is q . Solid circles denote matrix elements of the potentials from Eq. (2.18), $V_{\beta_1 \gamma_{13}}$ and $V_{\gamma_{13} \alpha_1}$, evaluated between two- and three-body states.

In Eq. (2.37), m_{α_1} is the mass of the one-body state $|\alpha_1 \mathbf{P}\rangle$, $V_{\alpha_1 \gamma_{12}}(k)$ is the vertex function of the potential V_{12} , $\tilde{V}_{\gamma_{12} \alpha_1}(k, E)$ is the vertex function for the dressed vertex \tilde{V}_{21} , $\tilde{G}_\gamma(k, E)$ is the dressed two-body Green function, and $a_{\gamma_{12}}(k, 0)$ is a factor from Eq. (2.33) associated with the phase space of the two-body system γ_{12} . The one-body mass counter term $\delta\Pi_\alpha$ is fixed by demanding that the elements of the one-body self-energies be identically zero when the driving energy $E = \mathcal{E}(m_{\alpha_1}, \mathbf{P})$. In the CM frame, the mass renormalization condition is

$$\text{Re}(\Pi_\alpha(E))_{E \rightarrow m_{\alpha_1}} = 0. \quad (2.38)$$

In this framework, the finite size of the hadrons involved results in vertex form factors, such as $V_{\beta_1 \gamma_{12}}(k)$, which fall off sufficiently rapidly with k to ensure the convergence of all integrals. Therefore, the counter terms $\delta\Pi$ and $\delta\Sigma$ are both finite.

Having obtained expressions for the dressed one- and two-body Green functions, one next considers the two-body scattering amplitudes $t^{(1)}$ and $t^{(2)}$. These scattering amplitudes depend on the one- and two-body Green functions, as well as the two-body kernel K . The two-body kernel is comprised of three contributions

$$K = K^{(1)} + K^{(2)} + K^{(4\text{pt})}, \quad (2.39)$$

where

$$K^{(1)} = V_{23}^{(2)} G_3 V_{32}^{(1)}, \quad (2.40)$$

$$K^{(2)} = V_{23}^{(1)} G_3 V_{32}^{(2)}, \quad (2.41)$$

and $K^{(4\text{pt})}$ is the part of the potential V_{22} that is *not* proportional to a Dirac δ -function in the relative momentum. This latter term is the direct four-point coupling of four mesons, and it is depicted as four meson lines converging on a single point in Fig. 1. In Eq. (2.39), the parenthetical superscripts on the first two quantities refer to which

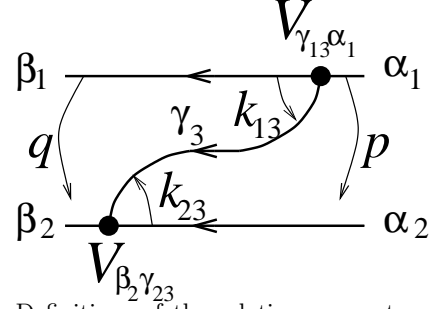


FIG. 6. Definitions of the relative momenta and particle labels for the kernel $K_{\beta\alpha}^{(1)}(q, p)$ given in Eq. (2.44).

of the two particles in the incoming state emits the exchanged particle, the superscript on the third quantity refers to the direct four-meson interaction. In the first two terms, the exchanged particle is subsequently absorbed by the other particle in the outgoing state.

Explicit expressions for the most general two-body kernels of Eqs. (2.40) and (2.41) in the spherical wave basis are complicated and not particularly enlightening. However, in the model application to $\pi\pi$ scattering considered in Sec. III, the resulting kernel is relatively simple. The only matrix elements of V_{23} that are of interest in this application are those associated with the transitions of the forms $\pi\pi \rightarrow \pi\pi\rho$, $\pi\pi \rightarrow \pi\pi f_0$, $\pi\pi \rightarrow K\bar{K}\rho$ and $\pi\pi \rightarrow K\bar{K}f_0$, $\pi\pi \rightarrow \pi\bar{K}K^*$. In each of these hadron states, at least two of the three particles are spin-0 mesons. For these interactions, the plane-wave matrix elements of the potentials $V_{23}^{(1)}$ are of the form

$$\begin{aligned} \langle \gamma_{123} \mathbf{K} \mathbf{k} \mathbf{k}_{13} | V_{32}^{(1)} | \alpha_{12} \mathbf{P} \mathbf{p} \rangle &= (2\pi)^3 \delta(\mathbf{K} - \mathbf{P}) \delta_{\gamma_2, \alpha_2} \\ &\times 2\mathcal{E}(m_{\alpha_2}, -\mathbf{p}) \\ &\times \langle \gamma_{13} \mathbf{k} \mathbf{k}_{13} | V_{21} | \alpha_1 \mathbf{p} \rangle, \end{aligned} \quad (2.42)$$

where the matrix elements of V_{12} are of the form

$$\begin{aligned} \langle \gamma_{13} \mathbf{k} \mathbf{k}_{13} | V_{21} | \alpha_1 \mathbf{p} \rangle &= (2\pi)^3 \delta(\mathbf{k} - \mathbf{p}) \frac{(-1)^{s_{\gamma_3} - \lambda}}{\sqrt{2s_{\gamma_3} + 1}} \\ &\sum_{\lambda} D_{\lambda \gamma_3, \lambda}^{s_{\gamma_3}}(-\mathbf{k}_{13}, \mathbf{p}) k_{13}^{s_{\gamma_3}} Y_{s_{\gamma_3}, -\lambda}^*(\hat{\mathbf{k}}_{13}) V_{\gamma_{13} \alpha_1}(k_{13}). \end{aligned} \quad (2.43)$$

The vertex for $V_{32}^{(1)}$ appears in Figs. 5 and 6 as the right-most interaction vertex. In the partial-wave basis, the kernel $K^{(1)}$ is shown in Fig. 6 and is given by

$$\begin{aligned} K_{\beta\alpha}^{(1)J}(q, p) &= 2\pi \sum_{\gamma_{123}} \int_{-1}^{+1} dx \frac{P_J(x)}{4\pi} \frac{1}{2\mathcal{E}(m_{\gamma_3}, \mathbf{p} - \mathbf{q})} \\ &\times \frac{V_{\beta_2 \gamma_{23}}(k_{23}) \mathcal{S}^{s_{\gamma_3}}(\mathbf{q}, \mathbf{p}) V_{\gamma_{13} \alpha_1}(k_{13})}{E - \mathcal{M}_{\gamma_{123}}(\mathbf{q}, -\mathbf{p}, \mathbf{p} - \mathbf{q}) + i\epsilon}, \end{aligned} \quad (2.44)$$

where

$$\begin{aligned} \mathcal{S}^{s_{\gamma_3}=0}(\mathbf{q}, \mathbf{p}) &= 1, \\ \mathcal{S}^{s_{\gamma_3}=1}(\mathbf{q}, \mathbf{p}) &= q_{\beta_1}^\mu \left(\frac{-m_{\gamma_3}^2 g_{\mu\nu} + k_{\gamma_3\mu} k_{\gamma_3\nu}}{\mathcal{M}_{\gamma_{23}}(k_{23}) \mathcal{M}_{\gamma_{13}}(k_{13})} \right) p_{\alpha_2}^\nu, \end{aligned} \quad (2.45)$$

for scalar exchanges ($s_{\gamma_3} = 0$) and vector exchanges ($s_{\gamma_3} = 1$), respectively, and $P_J(x)$ are the usual Legendre polynomials in $x = \mathbf{p} \cdot \mathbf{q} / pq$. The three four-momenta appearing in Eq. (2.44) are

$$\begin{aligned} q_{\beta_1}^\mu &= (\mathcal{E}(m_{\beta_1}, \mathbf{q}), \mathbf{q}), \\ p_{\alpha_2}^\mu &= (\mathcal{E}(m_{\alpha_2}, -\mathbf{p}), -\mathbf{p}), \\ k_{\gamma_3}^\mu &= (\mathcal{E}(m_{\gamma_3}, \mathbf{p} - \mathbf{q}), \mathbf{p} - \mathbf{q}). \end{aligned} \quad (2.46)$$

Expressions corresponding to the matrix elements of $K_{\beta\alpha}^{(2)}(q, p)$ can be obtained in a similar manner.

Once specific forms of the model vertex form factors $V_{\gamma_{13}\alpha_1}(k_{13})$ and $V_{\beta_2\gamma_{23}}(k_{23})$ are provided and substituted into Eq. (2.44), the matrix elements of the kernel K are computed numerically. One can proceed to solve the integral equation in Eq. (2.28) for the scattering amplitude $t^{(2)}$. In the CM frame, the integral equation for the partial-wave scattering amplitude $t_{\beta\alpha}^{(2)J}(q, p)$ has the form

$$\begin{aligned} t_{\beta\alpha}^{(2)J}(q, p) &= K_{\beta\alpha}^J(q, p) + \sum_{\gamma_{12}} \int_0^\infty dk a_{\gamma_{12}}(k, 0) \\ &\quad \times K_{\beta\gamma}^J(q, k) \tilde{G}_\gamma(k, E) t_{\gamma\alpha}^{(2)J}(k, p), \end{aligned} \quad (2.47)$$

where $a_{\gamma_{12}}(k, 0)$ is the usual two-body phase space factor. Obtaining the solution of this integral equation is complicated by the presence of the two-body pole in the two-body Green function $\tilde{G}_\gamma(k)$, and possibly the appearance of three-body unitarity cuts in both $\tilde{G}_\gamma(k)$ and the two-body kernel $K_{\beta\alpha}^J(q, p)$. The method used to solve this integral equation is adapted from Ref. [20]. It involves obtaining a two-body Moller operator $\Omega^{(2)}$, whose J^{th} partial-wave matrix element satisfies,

$$t_{\beta\alpha}^{(2)J}(q, p) = \sum_{\gamma_{12}} \int_0^\infty dk a_{\gamma_{12}}(k, 0) \Omega_{\beta\gamma}^{(2)J}(q, k) K_{\gamma\alpha}(k, p). \quad (2.48)$$

After a solution for $t_{\beta\alpha}^{(2)J}(q, p)$ is obtained, one proceeds to obtain an explicit expression for the two-body scattering amplitude $t^{(1)}$, which is given by Eq. (2.27). Since the solution of the intermediate dressed one-body Green function \tilde{G}_1 is obtained from the one-body self-energy from Eq. (2.37), all that remains is to determine the form of the dressed vertices \tilde{V}_{12} and \tilde{V}_{21} . The integral equation for the dressed vertex is obtained for the transpose of the dressed vertex from Eq. (2.25),

$$\begin{aligned} \tilde{V}_{\beta_{12}\alpha_1}(q) &= V_{\beta_{12}\alpha_1}(q) + \sum_{\gamma_{12}} \int_0^\infty dk a_{\gamma_{12}}(k, 0) \\ &\quad \times K_{\beta\gamma}^{J=s_{\alpha_1}}(q, k) \tilde{G}_\gamma(k, E) \tilde{V}_{\gamma_{12}\alpha_1}(k) \end{aligned} \quad (2.49)$$

The similarity between this integral equation and the integral equation of Eq. (2.47) with $J = s_{\alpha_1}$ which determines $t^{(2)}$ is clear. It follows that the solution to Eq. (2.49) is just

$$\tilde{V}_{\beta_{12}\alpha_1}(q) = \sum_{\gamma_{12}} \int_0^\infty dk a_{\gamma_{12}}(k, 0) \Omega_{\beta\gamma}^{(2)J=s_{\alpha_1}}(q, k) V_{\gamma_{12}\alpha_1}(k). \quad (2.50)$$

Finally, the two-body scattering amplitude $t^{(1)}$ is

$$t_{\beta\alpha}^{(1)J}(q, p) = \sum_{\gamma'_1\gamma_1} \frac{\tilde{V}_{\beta_{12}\gamma'_1}^J(q) \tilde{G}_{\gamma'_1\gamma_1}(E) \tilde{V}_{\gamma_1\alpha_{12}}^J(p)}{2\sqrt{m_{\gamma'_1}m_{\gamma_1}}} \quad (2.51)$$

The complete expression for the two-body scattering amplitude T_{22} is obtained by adding this expression for $t^{(1)}$ to $t^{(2)}$ according to Eq. (2.26).

In the previous sections, it was demonstrated that the explicit solution to the scattering problem involving one-, two-, and three-body states can be obtained by performing several integrations and one matrix inversion. The matrix inversion is necessary to obtain the two-body Moller amplitude $\Omega_{\beta\alpha}^{(2)J}(q, p)$.

III. APPLICATION TO $\pi\pi$ SCATTERING

In this section, the framework is applied to $\pi\pi$ scattering. Simple model forms of the elementary vertex form factors $V_{\beta_{12}\alpha_1}(q)$ are introduced, and solutions for the self-energies $\Pi_{\beta\alpha}(E)$ and $\Sigma_{\beta\alpha}(p, E)$ and scattering amplitudes $t_{\beta\alpha}^{(1)J}(q, p)$, $t_{\beta\alpha}^{(2)J}(q, p)$, and $\tilde{V}_{\beta_{12}\alpha_1}(q)$ are obtained numerically. Several interesting aspects of the obtained solutions are discussed. It should be emphasized that the model introduced in Sec. III A is preliminary and the manner in which the model parameters are fit to the data may be overly simplistic, as it focuses on reproducing only a few observables and therefore does not represent an exhaustive or complete study of the dynamics of $\pi\pi$ scattering. The motivation is to provide a demonstration of the framework and exhibit the features of the model, and its ability to describe the scattering of a system of strongly-coupled particles with emphasis on the multi-particle channel aspect. More complete studies of meson scattering within the present framework will be the subject of future articles.

In Sec. III A, the dynamical assumptions are discussed along with the model parameters. A detailed list of the states included in the Hilbert space is provided. The model parameters are determined using a simple method to fit experimental data for the $\pi\pi$ isoscalar-scalar phase shift and ρ -meson decay width, using the S -wave phase shifts from Ref. [21]. In Sec. III B the resulting phase shifts, inelasticities and cross sections are provided and compared to the data, and some aspects of the $f_0(980)$ scalar meson are discussed in terms of a $K\bar{K}$ bound state.

A. Dynamical model for $\pi\pi$ scattering

The model is intended to describe the scattering in a range of center-of-momentum (CM) energies from thresh-

old ($E = 2m_\pi \approx 280$ MeV) to about $E = 1400$ MeV. Above 1400 MeV, it is important to include in more detail the effects of the three scalar mesons observed in this region. For this preliminary study, however, it is possible to avoid making strong assumptions concerning these scalar mesons, hence the model will not be accurate in this energy region. In the following, only the isoscalar-scalar ($I = 0, J = 0$) and isovector-vector ($I = 1, J = 1$) channels are considered. The motivation is to explore some of the interesting physical aspects of the present framework and to estimate the importance of including three-body states in such a model of hadron scattering. The assumptions of the dynamical model are summarized below.

Two-body states: For the channels and energies explored herein, it is assumed that $\pi\pi$ scattering is primarily determined by the dynamics arising from the coupling of the $\pi\pi$ and $K\bar{K}$ two-body channels. Hence, $|\pi\pi\rangle$ and $|K\bar{K}\rangle$ are the only two-body channels included in the Hilbert space.

One-body states: It is assumed that the coupling of the $K\bar{K}$ system is strong enough to result in the appearance of a narrow resonance in the scalar-isoscalar channel at $E \approx 980$ MeV. This state is identified with the $J^{PC} = 0^{++}$ $f_0(980)$ meson. Since this scalar meson is presumed to arise from final-state interactions as a quasi-bound $K\bar{K}$ state, it is not part of the free Hilbert space, and there is no bare mass associated with it. Rather, it appears as a pole in the analytically-continued T -matrix. Furthermore, in the limit that the two-body $\pi\pi$ and $K\bar{K}$ channels decouple, this pole moves to the real-energy axis below the two-kaon threshold; that is, it becomes a $K\bar{K}$ bound state in this limit. The identification of the $f_0(980)$ meson as a $K\bar{K}$ molecule is controversial. Although it appears as a molecular state in this model, the “true” nature of the $f_0(980)$ meson remains an open question.

In contrast to the $f_0(980)$ meson, it is assumed that at least one of the scalar resonances observed in the mass region between 1300 and 1700 MeV will be a QCD bound state; that is, a state which arises as a bound state whose constituents are quarks, antiquarks and gluons. Such states do not arise from the meson final-state interactions, they are not bound states of mesons, and hence must be included in the model as *bare* states with bare masses.

Experiments reveal the presence of several resonances in the scalar-isoscalar channel between 1300 and 1700 MeV. A complete study of the $\pi\pi$ scattering system in this energy range requires the inclusion of each of these resonances into the model. However, to simplify the present study, all of these resonances are modeled in terms of a single scalar resonance. The resonance is assumed to have a mass of 1350 MeV, which gives it a mass similar to the lightest of the resonances above kaon threshold, referred to as the $J^{PC} = 0^{++}$ $f_0(1370)$ meson. One ramification of choosing a single scalar resonance to model the effect of all observed resonances in

TABLE I. Masses and widths of mesons. Masses that are underlined have been fixed to reproduce the accepted values. All other values are obtained from the model calculation. In the present study, the width of the K^* meson was not calculated. All values are given in units of MeV.

	π	K	ρ	K^*	$f_0(1350)$	$f_0(980)$
mass	<u>140</u>	<u>500</u>	<u>770</u>	<u>890</u>	<u>1350</u>	996
width	0	0	150	—	805	46

TABLE II. Isospin coupling constants for kernel $K_{\beta\alpha}(q, p)$ for isoscalar, S -wave ($I = 0, J^{PC} = 0^{++}$) and isovector, P -wave ($I = 1, J^{PC} = 1^{--}$) scattering.

Channel	Exchange	$I = 0, J = 0$	$I = 1, J = 1$
$\pi\pi \leftrightarrow \pi\pi$	$\pi\pi f_0$	1	1
$K\bar{K} \leftrightarrow K\bar{K}$	$K\bar{K} f_0$	1	1
$\pi\pi \leftrightarrow \pi\pi$	$\pi\pi\rho$	-1	-1
$K\bar{K} \leftrightarrow K\bar{K}$	$K\bar{K}\rho$	-1	-1
$\pi\pi \leftrightarrow K\bar{K}$	$\pi K K^*$	$-\sqrt{2}$	-1

the 1300–1700 MeV region, is in the width of this resonance. In order to fit the model parameters to the $\pi\pi$ phase shifts requires a single effective resonance with a very large width. It is found that the model resonance has a decay width of 805 MeV, which is approximately the *sum* of the widths of the three observed resonances in this region.

Three-body states: Only three-body states are included that can couple to the $\pi\pi$ or $K\bar{K}$ states through the absorption or emission of the isovector $J^{PC} = 1^{--}$ $\rho(770)$, isodoublet $J^P = 1^-$ $K^*(892)$, and $J^{PC} = 0^{++}$ f_0 mesons. Thus, the three-body states included in this study are $|\pi\pi\rho\rangle$, $|\pi\pi f_0\rangle$, $|K\bar{K}\rho\rangle$, $|K\bar{K} f_0\rangle$, $|\pi\bar{K} K^*\rangle$ and $|\pi K K^*\rangle$.

To summarize, the hadronic states included in this model of $\pi\pi$ scattering are

$$\begin{aligned}
&|f_0\rangle, |\rho\rangle, \\
&|\pi\pi\rangle, |K\bar{K}\rangle, \\
&|\pi\pi\rho\rangle, |K\bar{K}\rho\rangle, |\pi\bar{K} K^*\rangle, |\pi\pi f_0\rangle, |K\bar{K} f_0\rangle, \quad (3.1)
\end{aligned}$$

where the f_0 meson refers to the $f_0(1350)$ meson. (The $f_0(980)$ meson is expected to appear in the model as a $K\bar{K}$ resonance.) The values of the bare masses of these particles are provided in Table I and are underlined to indicate that they are input parameters. As discussed in Sec. II, one- and two-body counter terms are included in the elementary interaction potentials V_{11} and V_{22} , respectively, such that the bare masses given in Table I coincide with the dressed masses of the mesons.

Model vertex form factors: The vertices in the model are assumed to be finite-sized and hence require the appropriate form factors for the relative three-momentum \mathbf{q} . They are given by the universal form:

$$V_{\beta_1\beta_2\alpha_1}(q) = a_{\beta_1\beta_2\alpha_1} \sqrt{\frac{16\pi}{2s_{\max} + 1}} e^{-q^2/\Lambda_{\beta_1\beta_2\alpha_1}^2}, \quad (3.2)$$

where $s_{\max} = \max\{s_{\beta_1}, s_{\beta_2}, s_{\alpha_1}\}$ is the largest spin of the particles involved. In the present study $s = 0$ for vertices involving the f_0 meson, and $s = 1$ for vertices involving the ρ or K^* mesons. The vertex coupling constants $a_{\beta_1\beta_2\alpha_1}$ and form factor momentum scales $\Lambda_{\beta_1\beta_2\alpha_1}$ are chosen to provide a good fit to the data for the isoscalar-scalar $\pi\pi$ phase shift $\delta_{\pi\pi}$ and the ρ -meson decay width $\Gamma_{\rho\rightarrow\pi\pi} = 150$ MeV. The parameter search was limited in a number of ways. First, the various meson-exchange form factor scales $\Lambda_{\beta_1\beta_2\alpha_1}$ in Table III were all constrained to be the same value and less than 1 GeV. The direct four-meson couplings in Table IV were chosen to be one of two scales, the first was taken to be 125 MeV larger, and the second to be 125 MeV smaller than the meson-exchange scales in Table III. In the following, it is shown that the vector-exchange interactions contribute little to the observables considered. To reduce the number of parameters, the strength of the vector-exchange vertices were taken to be identically equal $a_{\pi\pi\rho} = a_{K\bar{K}\rho} = a_{\pi KK^*}$. The isospin factors that arise in a calculation of the meson-exchange kernels $K_{\beta\alpha}^J(q, p)$, such as in Eq. (2.44), are given in Table II.

Direct interactions: In addition to meson exchanges, it is important to include real-valued potentials that directly couple two pseudoscalar mesons to two pseudoscalar mesons, as a part of the $K^{(4\text{pt})}$ kernel in Eq. (2.39). Such interaction potentials could arise from the direct coupling of four mesons to a virtual-quark loop. Here, two direct four-point interactions are considered. The first is intended as a way to mimic some of the effects of dynamical chiral symmetry breaking. This interaction is taken to be of the form given by the elementary potential V_{22} and is referred to as the direct 4π (or $4K$) interaction. In a partial-wave basis, the form of the four-pion interaction is given by

$$K_{\pi\pi,\pi\pi}^{(4\pi)J}(q, p) = 16\pi (qp)^J a_{4\pi}^2 e^{-q^2/\Lambda_{4\pi}^2} e^{-p^2/\Lambda_{4\pi}^2}, \quad (3.3)$$

and the four-kaon term $K^{(4K)J}(q, p) = 0$. The second four-point interaction is a short-ranged attraction modeled as a t -channel exchange of a heavy scalar-isoscalar meson. Its form is given by the scalar-exchange kernel of Eq. (2.44) and the two-body self-energy Σ of Eq. (2.31). For simplicity it is treated exactly as if two additional three-body states,

$$|\pi\pi X\rangle, |K\bar{K} X\rangle, \quad (3.4)$$

with $m_X = 1500$ MeV, were added to the Hilbert space. Clearly, modelled in this manner, for energies $E > m_X + 2m_\pi = 1780$ MeV, the state $|\pi\pi X\rangle$ can go on-energy-shell. However, the calculations described herein are for energies less than 1400 MeV, so that $|\pi\pi X\rangle$ is never on-energy-shell.

Again, the objective is to study the framework developed in this paper. That is, it is interesting to assess the importance and possibility of including the dynamics

TABLE III. Coupling strengths and momentum scales for the vertex form factors. The values of the momentum scales are given in MeV.

$\beta_1\beta_2\alpha_1$	$\pi\pi f_0$	$K\bar{K} f_0$	$\pi\pi\rho$	$K\bar{K}\rho$	$K\pi K^*$
$a_{\beta_1\beta_2\alpha_1}$	12.4	5.08	20.0	20.0	20.0
$\Lambda_{\beta_1\beta_2\alpha_1}$	875	875	875	875	875

TABLE IV. Coupling strengths and momentum scales for the four-point meson interactions. The values of the momentum scales are given in MeV.

	$\pi\pi X$	$K\bar{K} X$	4π	$4K$
a	19.8	11.0	17.2	0.0
Λ	1000	1000	750	750

of three-body intermediate states to the study of meson scattering and final state interactions, rather than to test a particular interaction model for $\pi\pi$ scattering.

Once the forms of the model vertices are fixed, the only observables used in the fit are the scalar-isoscalar $\pi\pi$ phase shift $\delta_{\pi\pi}$, the existence of the $K\bar{K}$ resonance (referred to as the $f_0(980)$), and the decay width of the $\rho(770)$ vector meson. All measurable reaction channels are not used in the fitting procedure, since this paper represents more a proof of principle of the framework rather than a complete phenomenological analysis of $\pi\pi$ scattering. The resulting values of the coupling constants are provided in Tables III and IV.

B. Phase shifts and inelasticities

Below all three-body thresholds, the non-trivial part of the S -matrix in Eq. (2.16) can be written as a 2×2 unitary matrix $S_{\beta\alpha}(E)$ with α, β denoting the only two open channels $\pi\pi$ and $K\bar{K}$. The S -matrix in the J^{th} partial wave can be parametrized in terms of two phase shifts $\delta_{\pi\pi}$ and $\delta_{K\bar{K}}$, and one inelasticity $\eta_{\pi\pi}$,

$$\delta_\alpha(E) = \frac{-i}{2} \ln \frac{S_{\alpha\alpha}^J(E)}{\eta_\alpha(E)}, \quad (3.5)$$

$$\eta_\alpha(E) = |S_{\alpha\alpha}^J(E)|, \quad (3.6)$$

for $\alpha = \pi\pi, K\bar{K}$. Below all three-body thresholds there are only two stable channels, $\pi\pi$ and $K\bar{K}$. Hence, there is only one inelasticity parameter $\eta_{\pi\pi} = \eta_{K\bar{K}}$. For energies E above the lowest stable three-body threshold, one must augment the S -matrix by including all stable three-body states. Consequently, its parametrization requires more than two phase shifts and one inelasticity. Nonetheless, one may still use Eqs. (3.5) and (3.6) to define the phase shifts $\delta_\alpha(E)$, and inelasticities $\eta_\alpha(E)$ for the two channels $\alpha = \pi\pi$ and $K\bar{K}$. Of course, above the threshold of a stable three-body state $\eta_{\pi\pi} \neq \eta_{K\bar{K}}$.

The $\pi\pi$ phase shift, as defined by Eq. (3.5) and obtained from our model, is shown as a solid curve in Fig. 7.

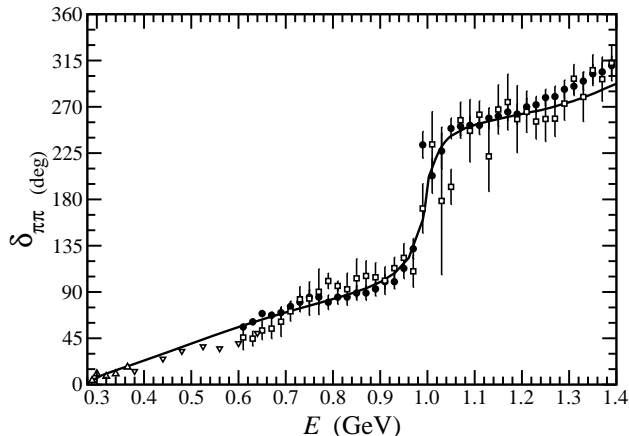


FIG. 7. The $\pi\pi$ scattering phase $\delta_{\pi\pi}$ in the scalar, isoscalar channel as a function of the CM driving energy E . The data are from Refs. [22] (open squares), [23] (closed circles), [24] (up triangles), and [25] (down triangles).

The model provides an excellent description of the $\pi\pi$ phase shift data depicted in Fig. 7 [22–25], and the inelasticity $\eta_{\pi\pi}$, as shown in Fig. 8. The overall trend of the pion scattering phase shift $\delta_{\pi\pi}$ is positive and increases slowly with energy E . This is indicative of a weak and attractive effective $\pi\pi$ scattering potential. At the kaon threshold, a rapid phase motion is apparent. It results from the presence of a narrow, $f_0(980)$ scalar meson. Above the two-kaon threshold, the phase shift continues to increase slowly, at a rate similar to the increase in the phase shift below the threshold.

Below all other thresholds, the $\pi\pi$ channel is the only open channel, and unitarity requires that the inelasticity $\eta_{\pi\pi} = 1$ here. This is clearly observed in Fig. 8, where the calculated inelasticity $\eta_{\pi\pi}$ has a value consistent with unity below the threshold of the $K\bar{K}$ channel at 1 GeV. Had four-body states been included into this framework, one might have expected to see a decrease in the inelasticity $\eta_{\pi\pi}$ due to the opening of the four-pion state, which has a threshold of $E = 4m_\pi \approx 0.560$ GeV. However, the data in Fig. 8 [22] seem to suggest that the contribution of the four-pion state to $\pi\pi$ scattering is negligible. This can be seen by noting the lack of any systematic deviation from $\eta_{\pi\pi} = 1$ for the range of energies $4m_\pi < E < 2m_K$.

It is clear from both Figs. 7 and 8 that the $K\bar{K}$ channel has a significant effect on $\pi\pi$ scattering. At the two-kaon threshold at $E \approx 1.0$ GeV, one observes a rapid increase in the $\pi\pi$ phase shift $\delta_{\pi\pi}$, and a sharp fall off of the $\pi\pi$ inelasticity $\eta_{\pi\pi}$ to its minimum value $\eta_{\pi\pi} \approx 0.31$. This phase motion is indicative of crossing the thresholds of the two-body $K\bar{K}$ state and the one-body $f_0(980)$ bound state. The rapid increase observed in the phase shift $\delta_{\pi\pi}(E)$ is due to the *weak* coupling between the $\pi\pi$ and $K\bar{K}$ channels. In the model, when the mixing of these two channels is further weakened, the rate of change of

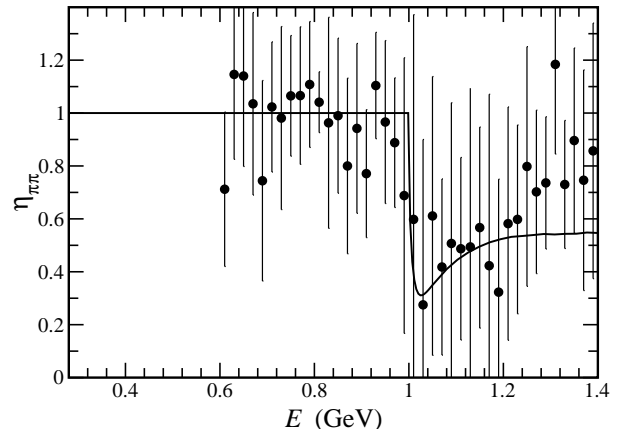


FIG. 8. The $\pi\pi$ scattering inelasticity $\eta_{\pi\pi}$ in the scalar, isoscalar channel as a function of the CM driving energy E . The data are from Ref. [22].

the phase motion tends to *increase*, until finally, in the limit that the coupling between the two channels goes to zero, the phase motion becomes a step-function of magnitude 180 degrees. Such a phase motion is completely unobservable, and could therefore be ignored altogether (although it is relevant to Levinson’s theorem, which relates overall changes in the phase shifts from threshold to infinite energy to the number of bound states in a system).

The importance of the coupling between the two-body channels $\pi\pi$ and $K\bar{K}$ can be estimated quantitatively by recalculating the pion phase shift $\delta_{\pi\pi}$ after removing the kaon state $|K\bar{K}\rangle$ from the Hilbert space. The result is shown as the dotted curve in Fig. 9. However, from the above argument, perhaps a better indication of the importance of the $K\bar{K}$ channel is obtained by letting the couplings that lead to a mixing between the $K\bar{K}$ and $\pi\pi$ channels go *smoothly* to zero. (In practice, this is done by not allowing the one-body scalar $f_0(1350)$ to have a bare coupling to the $K\bar{K}$ state, and setting $a_{K^*\pi K} = 0$. This has a minimal effect on the dynamics but prevents mixing the $|\pi\pi\rangle$ and $|K\bar{K}\rangle$ states.) In this limiting case, the two states $|K\bar{K}\rangle$ and $|f_0(980)\rangle$ are coupled to the $|\pi\pi\rangle$ state, but the contributions they make to $\pi\pi$ scattering go to zero. The result is that for energies $E > 1000$ MeV, the $\pi\pi$ scattering amplitude will cross the branch cuts associated with the opening of these two channels. But since these channels do not mix with the $\pi\pi$ channel in this limit, the $\pi\pi$ phase shift exhibits a step-like motion at $E = 1.0$ GeV. This is shown as the dashed curve in Fig. 9. The difference between the solid curve, which represents the full model calculation, and the dashed curve in Fig. 9 may be taken as being indicative of the significance of the $K\bar{K}$ channel on $\pi\pi$ scattering. One concludes that the mixing between the $\pi\pi$ and $K\bar{K}$ channels is significant near and below the two-kaon threshold, where it

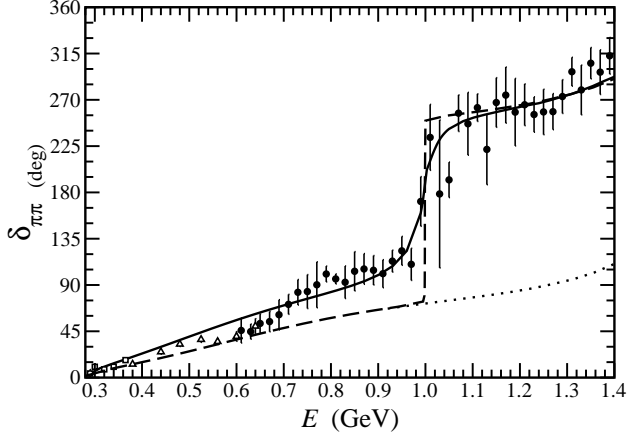


FIG. 9. The $\pi\pi$ scattering phase $\delta_{\pi\pi}$ in the scalar, isoscalar channel versus the CM energy E . The full calculation (solid curve) is compared to the calculation (dashed and dotted curves) in the limit the $K\bar{K}$ and $\pi\pi$ states become decoupled. The data are from Ref. [22].

can contribute more than half of the total phase shift $\delta_{\pi\pi}$. At energies above the two-kaon threshold, its importance quickly diminishes and vanishes altogether above $E = 1150$ MeV.

The importance of the mixing between the $\pi\pi$ and $K\bar{K}$ channels can also be observed in the pion inelasticity $\eta_{\pi\pi}$ shown in Fig. 8. Just above the two kaon threshold, the inelasticity plummets to a minimum value $\eta_{\pi\pi} \approx 0.31$. In the limit that the coupling to the kaon channel goes to zero, as described above, the inelasticity takes on a very different appearance.

In Fig. 10, the two pion inelasticity is plotted above the $K\bar{K}$ threshold. Below the threshold its value is unity. The lowest multi-particle state to which two-pion flux can be lost is the three-particle channel $|\pi\pi\rho\rangle$. The production threshold of this state is 1050 MeV. It is clear that one observes a slow decrease in the inelasticity $\eta_{\pi\pi}$ above 1050 MeV, due to the opening of the $\pi\pi\rho$ channel. The effect of this channel on the inelasticity is very small, with a minimum value $\eta_{\pi\pi} \approx 0.994$.

The energy dependence of the S -wave pion scattering inelasticity $\eta_{\pi\pi}$ and phase shift $\delta_{\pi\pi}$ are conveniently plotted together in an Argand diagram. In Fig. 11, the partial-wave scattering amplitude $a_{\pi\pi}^{J=0}(E)$ is plotted in the complex plane as a parametric function of the CM energy E . This figure clearly shows the rapid rise in the elastic $\pi\pi$ phase shift just below 1 GeV, and the resulting dramatic loss of flux from the elastic channel as soon as the $K\bar{K}$ channel opens up.

For spinless particles, the amplitude is given by

$$a_{\pi\pi}^J(E) = \frac{\eta_{\pi\pi} e^{2i\delta_{\pi\pi}} - 1}{2i}, \quad (3.7)$$

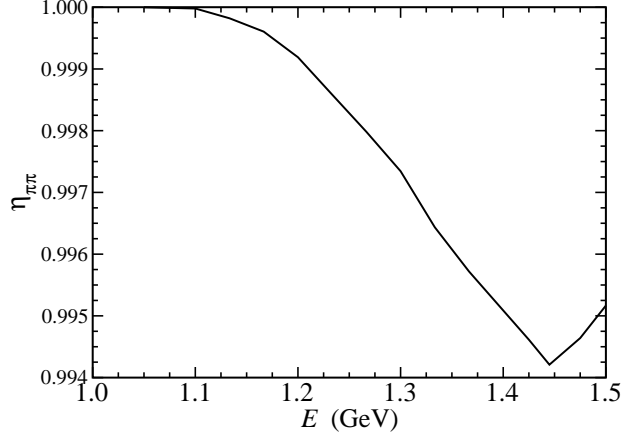


FIG. 10. The $\pi\pi$ inelasticity $\eta_{\pi\pi}$ in the isoscalar-scalar channel with no kaons.

$$= -\frac{p_0}{(4\pi)^2} \frac{1}{2E} z_{\pi\pi} \times \left(t_{\pi\pi, \pi\pi}^{(1)J}(p_0, p_0) + t_{\pi\pi, \pi\pi}^{(2)J}(p_0, p_0) \right), \quad (3.8)$$

where $p_0 = \sqrt{E^2/4 - m_{\pi\pi}^2}$ is the magnitude of the on-energy-shell three-momentum of the pions, $z_{\pi\pi}$ is the wave function renormalization of the two-pion state $|\pi\pi\rangle$, and $t_{\beta\alpha}^{(1)J}(q, p)$ and $t_{\beta\alpha}^{(2)J}(q, p)$ are the two-body scattering amplitudes, obtained from Eqs. (2.47) and (2.51), respectively. The two-body scattering cross section $\sigma_{\beta\leftarrow\alpha}(E)$ can be written in terms of the partial-wave scattering cross sections according to

$$\sigma_{\beta\leftarrow\alpha}(E) = \sum_{J=0}^{\infty} \sigma_{\beta\leftarrow\alpha}^J(E). \quad (3.9)$$

In terms of the scattering amplitudes, these partial-wave cross sections are given by

$$\sigma_{\beta\leftarrow\alpha}^J(E) = \frac{2J+1}{4\pi} \frac{z_{\beta} z_{\alpha}}{64\pi^2 E^2} \left| t_{\beta\alpha}^{(1)J}(q_0, p_0) + t_{\beta\alpha}^{(2)J}(q_0, p_0) \right|^2, \quad (3.10)$$

where p_0 and q_0 are the on-energy-shell solutions to $\mathcal{M}_{\alpha}(p_0) = E$ and $\mathcal{M}_{\beta}(q_0) = E$, respectively. The resulting cross section for elastic, S -wave $\pi\pi$ scattering is shown as a solid curve in Fig. 12. It is finite at threshold, exhibits a maximum value of 43 millibarns at $E \approx 600$ MeV, and a sharp decrease at the position of the $f_0(980)$ scalar meson resonance. This sudden drop occurs just below the $K\bar{K}$ threshold, as can be seen upon examination of the inset plot in Fig. 12 which depicts a closeup of the $K\bar{K}$ threshold region.

The dot-dashed curve is the resulting cross section $\sigma_{K\bar{K}\leftarrow\pi\pi}^{J=0}$ for the two-kaon production process $\pi\pi \rightarrow K\bar{K}$. This cross section is considerably smaller than that of the

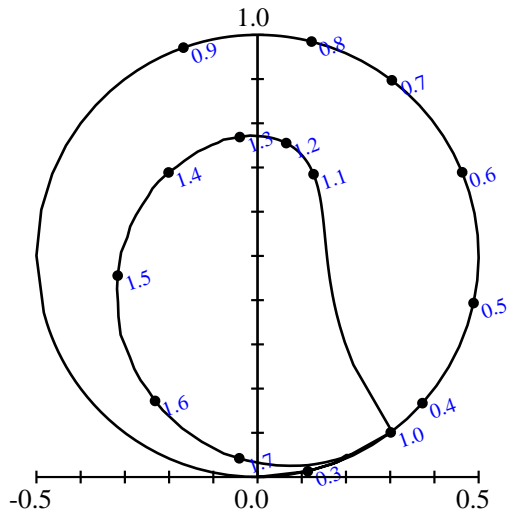


FIG. 11. Argand diagram for $\pi\pi$ scattering at all energies. Plotted is the energy dependence of the real and imaginary parts of the partial-wave scattering amplitude $a_{\pi\pi}^{J=0}(E)$ for the $J=0$ partial wave from Eq. (3.7) or Eq. (3.8). The curve is calculated for all energies $E > 2m_\pi$, and annotated with the corresponding energies E in GeV, from threshold to above $E = 1.7$ GeV.

elastic $\pi\pi$ scattering cross section, reaching its maximum value of 4.6 millibarns just above the two-kaon threshold at $E = 1$ GeV. Its small size is a result of the weak coupling between the two-pion and two-kaon channels. As discussed above, a weak coupling of these channels is necessary to ensure a narrow $f_0(980)$ meson. If the mixing between the pion and kaon channels were stronger, the $f_0(980)$ meson would more easily decay into two pions, tending to increase its width significantly.

The dashed curve in Fig. 12 is the S -wave cross section for elastic $K\bar{K}$ scattering. This cross section is comparably huge, having its maximum at the two-kaon threshold energy. Its size can be compared to that of the two-pion elastic cross section,

$$\begin{aligned}\sigma_{\pi\pi\leftarrow\pi\pi}^{J=0}(E=2m_\pi) &\approx 18.3 \text{ mb}, \\ \sigma_{K\bar{K}\leftarrow K\bar{K}}^{J=0}(E=2m_K) &\approx 734 \text{ mb}.\end{aligned}$$

The very large $K\bar{K}$ cross section arises from the scalar $f_0(980)$ meson which lies just below the $K\bar{K}$. The presence of a bound state just below the two-body scattering threshold will generally tend to increase the size of the cross section dramatically.

As was discussed earlier in Sec. III A, the model parameters were chosen to provide a good fit to the S -wave pion phase shift $\delta_{\pi\pi}$ data from Ref. [21]. In Fig. 7, the resulting phase shifts are also in excellent agreement with the data analyses of Ref. [22], [24], and [25]. However, it is important to realize that direct comparison of these model results with these $\pi\pi$ scattering data must be done with caution. Extraction of these data requires the use

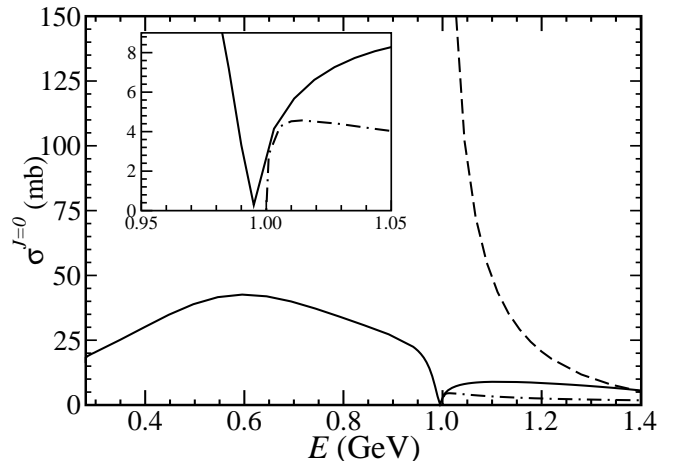


FIG. 12. S -wave cross section $\sigma^{J=0}(E)$ in millibarns for $\pi\pi \rightarrow \pi\pi$ (solid curve), $K\bar{K} \rightarrow K\bar{K}$ (dashed curve), and $\pi\pi \rightarrow K\bar{K}$ (dot-dashed curve). The inset shows a detail of the region around the $K\bar{K}$ threshold at $E = 1$ GeV.

of theoretical models, or theoretical assumptions, in order to fit the experimental observables. In the worst-case scenario, the resulting $\pi\pi$ phase shift data may be more representative of the extraction methods employed than of the actual $\pi\pi$ scattering process.

The extraction of the $\pi\pi$ phase shifts from experiment is a difficult and long-standing problem of hadron physics. At present, it is impossible to construct an experiment in which a pion beam is scattered from a pion target. Hence, other techniques are required to extract the $\pi\pi$ phase shift from experimental observables. One possibility is to use decays that produce two pions in the final state, and attempt to extract the $\pi\pi$ phase shifts from the final-state interactions.

The procedure employed by Ref. [24] is extract the phase shifts from the electroweak kaon decay $K^+ \rightarrow \pi^+\pi^0 e^+\nu_e$. The results are shown as open squares in Figs. 9 and 13. Extraction of the phase shift using decays with more than two particles in the final state requires some knowledge of transition form factors for the coupling of a kaon, two pions and the W boson to determine $K^+ \rightarrow \pi^+\pi^-W^+$. A nice feature of employing the electroweak decay $K^+ \rightarrow \pi^+\pi^0 e^+\nu_e$ is that the two pions are the only strongly-interacting particles in the final state. Hence, one would expect that the $\pi\pi$ interactions would be the dominant contribution to the dressing of the final state. However, this approach is hampered by two experimental difficulties. The first is the lack of statistics. This particular kaon decay represents only a small fraction (4×10^{-5}) of the total K^+ -meson decay width, which is already extremely small. The second is the fact that the energies and angles of the outgoing leptons provide a small lever arm with which to vary the CM energy E of the two final-state pions.

Another method is to extract the final state interactions of the two-pion production process $\pi p \rightarrow \pi\pi n$, employed by Ref. [25] (down triangles), Ref. [22] (open squares), and Ref. [23] (closed circles), shown in Fig. 7. These studies require some theoretical input in order to perform the extraction of the $\pi\pi$ scattering phase shift $\delta_{\pi\pi}$ and inelasticity $\eta_{\pi\pi}$; hence, they are not direct measurements of the $\pi\pi$ scattering phase shift.

Our model parameters were originally fit to the $\pi\pi$ phase shifts obtained by an analysis [23] of an experiment at CERN involving $\pi^- p \rightarrow \pi^+ \pi^- n$ at 17.2 GeV. Recently, this same data was re-examined by Kaminski *et al.* [22], with weaker model assumptions than were used in Ref. [23]. The work of Ref. [22] provides an exhaustive and *nearly* complete study of the $\pi\pi$ phase shift. In particular, there is no assumption that pion exchange is the dominant mechanism for the process $\pi^- p \rightarrow \pi^+ \pi^- n$. Consequently, this analysis seems to be more general than the others. A relative phase ambiguity in the analysis of Ref. [22] provides four possible, distinct solutions for the $\pi\pi$ phase shifts and inelasticities. Two of these solutions seem to have an unphysical inelasticity $\eta_{\pi\pi}$ below the two-kaon threshold and can be discarded. The other two solutions, denoted the “up-flat” and “down-flat” solutions, are very similar in appearance and neither can be dismissed on qualitative grounds. The phase shifts from the “down-flat” solution of Ref. [22] are shown as solid circles in Figs. 9 and 13.

The general behavior of the $\pi\pi$ phase shift $\delta_{\pi\pi}$ is positive, which is indicative of an attractive $\pi\pi$ scattering amplitude. An abrupt increase in the pion phase shift is evident at 1 GeV, which is due to the combined effects of the opening of the $K\bar{K}$ threshold and the crossing of the scalar $f_0(980)$ resonance.

Apart from this feature, which in this particular model is a result of the delicate mixing between the $\pi\pi$ and $K\bar{K}$ channels, the calculated pion phase shift $\delta_{\pi\pi}$ exhibits a steady, gentle increase from the threshold at 280 MeV to above 1400 MeV! In the model, this slowly increasing behavior arises from subtle cancellations between the attractive potentials of the heavy scalar-meson exchanges and the repulsive, direct four-pion interaction from Eq. (3.3) which is intended to model the effect of dynamical chiral symmetry breaking. The different form factor scales involved in these interactions (see Tables III and IV) are chosen to provide this slowly increasing, weak phase shift observed in the two-pion channel. Typically, scalar potentials by themselves provide a strong attraction in the S -wave $\pi\pi$ channel, that leads to a rapidly rising phase shift just above the $\pi\pi$ threshold, which then quickly falls away. This behavior is not seen in the $\pi\pi$ phase shift $\delta_{\pi\pi}$.

The importance and role of the scalar resonances in $\pi\pi$ scattering can be appreciated by a close examination of Fig. 13. The effect of the heavy s -channel resonances which are collectively modeled by the single $f_0(1350)$ in the model is two fold. First, their presence leads to a strong attractive potential for energies below 1400 MeV.

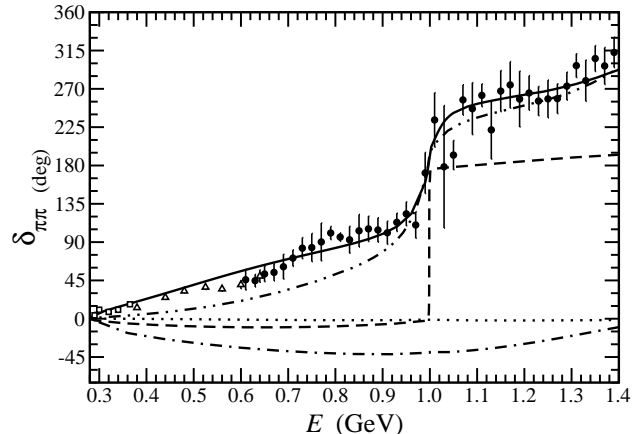


FIG. 13. Importance of the different model contributions to $\pi\pi$ scattering phase shift. The solid curve is the full calculation. The dashed curve is obtained by removing the one-body state $f_0(1350)$ from the Hilbert space. The dot-dashed curve is obtained by completely removing the scalar $f_0(1350)$ from the theory, both in one-body and three-body states. The dotted curve is same as the dot-dashed curve, but all scalar couplings (the “X”-exchanges and contact terms) are also set to zero. This is the effect of just the vector-meson exchanges. Above threshold it is negative with a minimum of $\delta_{\pi\pi} \approx -2.0$ degrees at $E \approx 1.2$ GeV. The dot-dot-dashed curve is obtained by weakening the coupling of the one-body $f_0(1350)$ state to the $\pi\pi$ state by 10 percent. The data points are from Fig. 7.

Second, they provide the most important contribution to *off-diagonal* matrix elements of the two-body scattering kernel K . That is, they provide the strongest source of mixing for the two-pion and two-kaon states in this model.

Both of these effects tend to produce an attraction for the two pions. In particular, the strong attraction necessary to bind the kaons to form the $f_0(980)$ resonance results in a strong attraction in the two-pion channel as well. The amount of mixing between the two-pion and two-kaon states dictates the attraction felt by the pions. Hence, when the coupling between $|\pi\pi\rangle$ and $|f_0(1350)\rangle$ states is artificially reduced by as little as 10%, the result is significant, as shown by the dot-dot-dashed curve in Fig. 13. When the one-body state $|f_0(1350)\rangle$ is removed entirely from the Hilbert space, the result is the dashed curve. The resulting pion phase shift is negative and close to zero below the two-kaon threshold, and positive above the threshold. The absence of the one-body s -channel state $f_0(1350)$ reduces the mixing between the two-pion and two-kaon states, which results in a nearly stable (and very narrow) kaon bound state $f_0(980)$. In this case, one observes a $f_0(980)$ bound state with a width that has been reduced from 46 MeV to 0.28 MeV! This is a result of the fact that the $f_0 \rightarrow \pi\pi$ decay must proceed

through K^* exchange in the kernel K , which provides only a weak mixing of the $\pi\pi$ and $K\bar{K}$ states.

When all scalar mesons are removed from the theory entirely; that is, when the couplings that lead to the existence of one-body states $|f_0(1350)\rangle$, and three-body states $|f_0\pi\pi\rangle$ and $|f_0K\bar{K}\rangle$ are set to zero $a_{\pi\pi f_0} = a_{K\bar{K}f_0} = 0$, the resulting phase shift is shown in Fig. 13 by the dot-dashed curve. The slightly repulsive behavior is a result of the combined effect of the attractive scalar- X and repulsive four-point interactions associated with chiral symmetry, given by the parameters in Table IV.

To minimize the number of free parameters all of the couplings to vector mesons are chosen to be equal to each other $a_{\pi\pi\rho} = a_{K\bar{K}\rho} = a_{\pi K\bar{K}^*}$. These coupling strengths were then determined by solving P -wave $\pi\pi$ scattering at the ρ meson mass $E = m_\rho = 770$ MeV, and requiring that the ρ -meson width reproduced the experimental value $\Gamma_\rho = 150$ MeV, as given in Table I. It is found that the resulting coupling strength leads to a vector-meson exchange interaction kernel K which provides a very weak repulsion for $\pi\pi$ scattering. This is illustrated by the dotted curve in Fig. 13, where all of the couplings except those involving the vector mesons ($a_{\rho\pi\pi}$, $a_{\rho K\bar{K}}$, $a_{K^*\pi\bar{K}}$) are set to zero. The resulting phase shift is negative (repulsive) and very small; its largest absolute value is about 2 degrees. Thus, in this model, ρ -meson exchange is negligible in the S wave. This model differs from the analysis of Ref. [14], in which they report that the attractive potential (which leads to the binding of the $K\bar{K}$ into the $f_0(980)$ resonance) is primarily due to ρ -meson exchange, which is strong and attractive in their model. In the framework, the exchange of a spin-1 meson in the kernel K results in a very weak and mildly repulsive interaction. This difference is a result of how the spin couplings and energy denominators of the meson-exchange propagators are implemented in the kernels of the two frameworks.

Before ending this section, a final comment concerning the accuracy of the numerical methods employed is provided. The accuracy is measured using the unitarity condition (or optical theorem),

$$T - T^\dagger = T^\dagger(G - G^\dagger)T, \quad (3.11)$$

which is derived from the fact that V in Eq. (2.18) is Hermitian. Evaluating Eq. (3.11) between two-pion states, one obtains an equation that relates the two-pion flux missing from the *forward* direction to the one-, two-, and three-body outgoing flux observed leaving the scattering center. This relation provides a sensitive check of the numerical methods employed.

The fraction of lost two-pion flux observed as outgoing two- or three-particle states is shown versus the exponent a of the adiabatic scale $\epsilon = 10^{-a}$ GeV in Fig. 14 for CM energy $E = 1400$ GeV. For any energy E greater than the two-pion scattering threshold, there can be no stable one-particle state. It follows that no one-particle outgoing flux can be observed. In Fig. 14, the regions

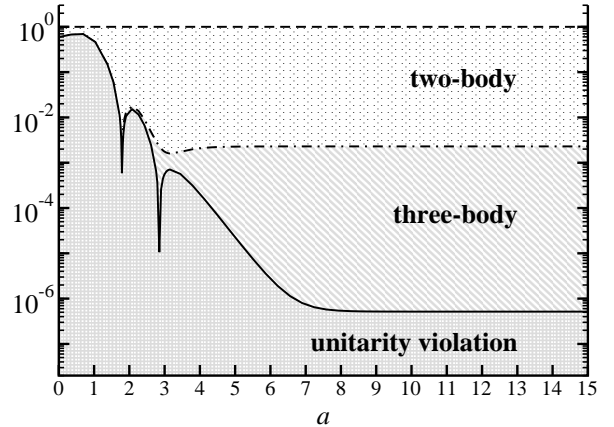


FIG. 14. Fraction of incoming two-pion flux at energy $E = 1400$ MeV in the isoscalar-scalar channel, appearing as “two-body” or “three-body” final states, or lost to unitarity violations. The fractions are shown versus the exponent a of the adiabatic scale $\epsilon = 10^{-a}$ GeV.

labeled “two-body” and “three-body” represent the fractions of the missing two-pion flux that appear as outgoing two-body ($\pi\pi$ or $K\bar{K}$) and three-body ($\pi\pi\rho$) states, respectively. Since the Hilbert space is restricted to one-, two- and three-body states, this should account for all the flux. However, in practice, the numerical methods employed introduce violations to the unitarity condition of Eq. (3.11). The region below the solid curve in Fig. 14 represents the fraction of flux that completely disappears from the theory; such a loss of flux violates unitarity. One observes that for values of $\epsilon \leq 10^{-7}$ GeV, the violation is less than 10^{-6} of the outgoing flux and is therefore negligible. In the application to $\pi\pi$ scattering described above, the value of $\epsilon = 10^{-12}$ GeV (or $a = 12$) was employed.

IV. SUMMARY AND FUTURE DIRECTIONS

Herein, a framework suitable for the description of non-perturbative hadron scattering, based on the Bakamjian-Thomas formulation of relativistic quantum mechanics is introduced. In Sec. II, it is shown that by including the interactions into the free mass operator \mathcal{M} , one can ensure that observables calculated in the framework are Lorentz covariant. When the Hilbert space is truncated to contain only one-, two- and three-body states, the resulting Lippmann-Schwinger equations (LSEs) form a closed set of coupled integral equations. The solution of these integral equations is obtained numerically.

A significant improvement of this framework over earlier work is that the *full* effect of three-body states have been included. The three-body Green functions appear only in the two-body scattering kernel K and the two-

body self-energy Σ , and for energies E above the three-body thresholds, unitary branch cuts associated with these thresholds appear both in K and Σ . It follows that the kernel K and two-body self-energy Σ are *complex* functions of the energy E . The appearance of such three-body branch cuts provides the means for important dynamical effects, such as three-hadron production and decays into three-hadron states, which are automatically accounted for in our framework. Such effects have hitherto been ignored for the most part in previous studies.

The inclusion of three-body cuts into the integral equations requires appropriate numerical methods to be employed. These methods, necessary to solve the coupled set of LSEs are shown to maintain the unitarity of the theory to better than one part in one million. To demonstrate the utility of the framework, a preliminary study of $\pi\pi$ scattering is carried out in Sec. III. The simple model, introduced in Sec. III A, is able to provide an excellent description of the $\pi\pi$ phase shifts and inelasticities.

The main purpose for developing this framework is to provide a means of incorporating the dynamics of low-momentum transfer, final-state interactions into the study of hadronic processes for energies up to a couple of GeV. In this energy region, the comparison between experimental data and theoretical predictions from models of QCD for quark and gluon dynamics, are often made difficult due to the presence of final-state interactions. The soft rescattering of final-state hadrons tends to *mask* the QCD dynamics of interest. The framework developed herein provides a tractable means to incorporate the effects of final-state interactions into studies of hadronic phenomena.

Towards this end, the framework is constructed to be a consistent extension for the constituent quark model. It provides a means to *unquench* the quark model by providing for hadron loops, multi-particle thresholds and the unitarity branch cuts associated with these. The result is the generation of complex-valued scattering amplitudes. It is an extension of the quark model, in that the quark model may be used to provide the elementary couplings and form factors for the hadronic interactions in V . The framework uses this real potential V to generate the full scattering solution.

Future applications of the framework will focus on the dynamics of nucleon resonances and exotic, hybrid mesons that are the subject of current and proposed experiments at TJNAF. In the baryon case, for energies up to about 2 GeV, there are some well-known and striking examples in πN scattering for which three-body effects are crucial in understanding the experimental observables. For example, in the $L_{2I,2J} = P_{11}$ channel, the πN inelasticity arising from the three-body $\pi\pi N$ state is very large [1]. It is likely that a complete understanding of the P_{11} πN scattering channel and the mysterious $N^*(1440)$ resonance requires the full implementation of three-body unitary cuts that this framework provides.

The effect of three-body cuts in exotic partial waves can also be very important. Most theoretical studies of

hybrid meson decays have so far ignored effects of final state interactions. The best candidate for the exotic meson, the $\pi_1(1600)$ [26] was found in the $\rho\pi$ decay channel, which is predicted to be suppressed with respect to other two body decay channels, in particular the $b_1\pi$ [27,28]. This shift of strength from $b_1\pi$ to $\rho\pi$ could be explained by mixing with the three-body, $\omega\pi\pi$ intermediate state which is believed to have a strong coupling to these two-meson channels.

ACKNOWLEDGMENTS

This work is supported by the U.S. Department of Energy under contract DE-FG02-87ER40365 and the National Science Foundation under contract PHY0070368.

-
- [1] J. A. Johnstone and T.-S. H. Lee, Phys. Rev. **C34**, 243 (1986).
 - [2] R. Jaffe, Phys. Rev. D **15**, 267 (1977).
 - [3] J. Weinstein and N. Isgur, Phys. Rev. D **27**, 588 (1983).
 - [4] T. Barnes, Phys. Lett. **B165**, 434 (1985).
 - [5] D. Morgan and M. R. Pennington, Phys. Lett. **B258**, 444 (1991).
 - [6] J. A. Oller, E. Oset, and J. R. Pelaez, Phys. Rev. Lett. **80**, 3452 (1998).
 - [7] E. Klempt, B. C. Metsch, C. R. Munz, and H. R. Petry, Phys. Lett. **B361**, 160 (1995).
 - [8] N. N. Achasov and G. N. Shestakov, Usp. Fiz. Nauk. **161**, 53 (1991).
 - [9] Particle Data Group, Eur. Phys. J. C **15**, 1 (2000).
 - [10] C. J. Morningstar and M. J. Peardon, Phys. Rev. D **60**, 034509 (1999); G. S. Bali *et al.* [SESAM Collaboration], Nucl. Phys. Proc. Suppl. **53**, 239 (1997)
 - [11] S. Narison, Nucl. Phys. **B509**, 312 (1998)
 - [12] P. Minkowski and W. Ochs, Eur. Phys. J. **C9**, 283 (1999)
 - [13] R. Kaminski, L. Lesniak, and B. Loiseau, Eur. Phys. J. **C9**, 141 (1999)
 - [14] G. Janssen, B. C. Pearce, K. Holinde, and J. Speth, Phys. Rev. **D52**, 2690 (1995).
 - [15] R. Kaminski, L. Lesniak, and J.-P. Maillet, Phys. Rev. **D50**, 3145 (1994).
 - [16] R. Kaminski, L. Lesniak, B. Loiseau, Phys. Lett. **B413**, 130 (1997).
 - [17] B. Bakamjian and L. H. Thomas, Phys. Rev. **92**, 1300 (1953).
 - [18] M. Betz and F. Coester, Phys. Rev. **C21**, 2505 (1980).
 - [19] M. A. Pichowsky, S. Walawalkar, and S. Capstick, Phys. Rev. **D60**, 054030 (1999).
 - [20] M. I. Haftel and F. Tabakin, Nucl. Phys. **158**, 1 (1970).
 - [21] B. R. Martin, D. Morgan, and G. Shaw, in "Pion-Pion Interactions in Particle Physics" (Academic, London, 1976), pp. 87-101, and references therein.
 - [22] R. Kaminski, L. Lesniak, and K. Rybicki, Acta. Phys. Polon. **B31**, 895 (2000).
 - [23] G. Grayer, et al., Nucl. Phys. **B75**, 189 (1974).
 - [24] L. Rosset, et al., Phys. Rev. **D15**, 574 (1977).

- [25] V. Shrinivasan et al., Phys. Rev. **D12**, 681 (1975).
- [26] G. S. Adams *et al.* [E852 Collaboration], Phys. Rev. Lett. **81**, 5760 (1998).
- [27] N. Isgur, R. Kokoski and J. Paton, Phys. Rev. Lett. **54**, 869 (1985).
- [28] P. Page, E. S. Swanson, and A. P. Szczepaniak, Phys. Rev. **D59**, 034016 (1999).